Article

Health Monitoring of Lithium-Ion Batteries Using Dual Filters

Richard Bustos [1], Stephen Andrew Gadsden [2,*], Pawel Malysz [3], Mohammad Al-Shabi [4] and Shohel Mahmud [1]

[1] College of Engineering and Physical Sciences, University of Guelph, Guelph, ON N1G 2W1, Canada; rbustos@uoguelph.ca (R.B.); smahmud@uoguelph.ca (S.M.)

[2] Department of Mechanical Engineering, McMaster University, Hamilton, ON L8S 4L8, Canada

[3] Department of Electrical and Computer Engineering, McMaster University, Hamilton, ON L8S 4L8, Canada; malyszp@mcmaster.ca

[4] Department of Mechanical and Nuclear Engineering, University of Sharjah, Sharjah, United Arab Emirates; malshabi@sharjah.ac.ae

* Correspondence: gadsden@mcmaster.ca

Abstract: Accurate estimation of a battery's capacity is critical for determining its state of health (SOH) and retirement, as well as to ensure its reliable operation. In this paper, a dual filter architecture using the Kalman filter (KF) and the novel sliding innovation filter (SIF) was implemented to estimate the capacity and state of charge (SOC) of a lithium-ion battery. NASA's Prognostic Center of Excellence (PCOE) B005 battery data set was selected for this experiment based on its wide use in academia and industry. This dataset contains cycling data of a 2 Ah lithium-ion battery until its capacity was measured at 1.3 Ah or less. The dual polarity equivalent circuit model (DP-ECM) was selected for modeling. The model parameter values were estimated using the least squares (LS) algorithm. Under normal operating conditions, both the dual-KF and dual-SIF performed similarly in terms of estimation accuracy. However, an uncertainty case was considered where the filters were subjected to rapid changing dynamics by cutting the data by 300 cycles. In this case, the battery capacity root-mean-square error (RMSE) for the dual-KF and the proposed dual-SIF were 0.1233 and 0.0675, respectively. Under rapidly changing dynamics and faulty conditions, the dual-SIF shows better convergence and robustness to disturbances.

Keywords: lithium battery; Kalman filter; dual Kalman filter; sliding innovation filter; state of charge; state of health; battery retirement

1. Introduction

In today's environmental movement towards greener technologies, lithium-ion batteries (LiBs) have become a popular solution for portable energy storage devices across all consumer electronics. Their high popularity can easily be attributed to the LiB's specific energy per weight [1]. LiBs provide a vast amount of energy while adding little weight to the system. However, great challenges are faced when implementing this technology, due to the LiB's high nonlinear nature [2]. Currently, LiBs have been extended to electric vehicle (EV) technology. In EVs, the battery is subject to aggressive current profiles, requiring a robust monitoring system to allow for their safe implementation [3].

A battery monitoring system (BMS) ensures the battery operates within the desired current, temperature, and voltage values [4]. Each LiB chemistry has a safe operating window bounded by specific limits of current, temperature, and voltage. Violation of any boundary can significantly reduce the battery's life or cause failure [5]. A key feature of the BMS is the accurate monitoring of the battery's SOC to prevent over discharging the battery while in operation [6]. SOC typically refers to the available amount of charge in the battery at any given time during usage, often displayed as a percentage value. Due to the LiB's dynamics and structure, SOC cannot be measured directly; hence, it must be estimated using indirect measurements such as voltage, current, and temperature [7]. In

the literature, some techniques to estimate SOC include the discharge test, ampere-hour counting, open circuit voltage (OCV), impedance spectroscopy, and implementation of signal processing techniques such as Kalman filters (KF) [8–11]. Most of these methods yield accurate SOC readings; however, it requires the battery to be offline, be in a laboratory setting, or destroys the battery in the process [9].

Modified versions of the ampere-hour counting method are the most common techniques to estimate for SOC [9]. The ampere-hour counting method is based on the relationship between the current input and the remaining capacity of the battery. If the initial SOC is known one may add/subtract based on the supplied/demanded current to the battery. However, its high dependency on the initial SOC, potential to accumulate sensor error and unknown current losses renders this method unreliable if it is not calibrated often [12,13]. A minimum voltage-based correction is often used by look-up table gains or computed using KFs and derivatives. Moreover, the battery is subject to aggressive current profiles causing its maximum capacity to degrade overtime. Estimation algorithms such as the KF provide a reliable strategy that yields accurate SOC estimates by making use of a battery model and available sensor readings such as the terminal voltage of the battery and demanded current [9,14].

The most popular battery models found in the literature are the electrochemical and equivalent circuit models (ECM) [15]. Electrochemical models are based on the underlying physics of the battery making use of complex partial differential equations, thus resulting in long running times and requiring high computational power [16]. On the other hand, ECMs have a simplistic mathematical structure that make use of electric elements such as resistors, capacitors, and voltage sources to model the dynamics of the LiB [17]. ECMs require low computational power and have low runtimes making them suitable for online applications.

The use of battery models, however, creates the need to accurately determine the values of the parameters in the model. For ECMs there are three main parameters to be determined which are a voltage source, a resistor, and resistor-capacitor (RC) branches which represents the LiB's open-circuit voltage (OCV), internal resistance, and transient responses, respectively [18].

The voltage source is represented by a curve that can be derived using a relationship between the OCV and SOC. To obtain the curve, the LiB is discharged using constant or pulse currents and let to rest, taking several hours to complete the experiment [19]. Different methods have been studied to determine the internal resistance and RC values. One method uses electrochemical impedance spectroscopy (EIS) data to derive the resistance and RC parameters in ECMs [20]. Several parameter identification techniques had been implemented using current-voltage (Input-Output) data such as neural networks (NN), least squares (LS), and grey box modeling [21–24]. Some of these techniques have long runtimes or require data to be gathered beforehand, making them suitable for offline implementation. To address this issue, some online techniques have been explored which include simplified versions of the NN and LS techniques. Other methods include Kalman filtering techniques which make use of a LiB parameter model that defines the parameters as states. The states of the parameter model are perturbed lightly to allow for their value to change throughout time [25].

In the literature, dual filters and joint methods have been studied to estimate for both the model's parameters and the states of the battery. In a joint KF strategy, the system matrix is augmented to include the parameter states, resulting in a larger matrix [26]. On the other hand, dual filters break the estimation process into two filters, one for the battery states and one for parameter estimation. Dual filters present several computational advantages as they make use of smaller matrices. Dual filters can track changes of the battery's internal resistance and maximum capacity [27]. Tracking maximum capacity can be used to estimate the current state of health (SOH) of the battery and allow for an accurate method to determine battery retirement—often when the LiB's maximum capacity is at 80% compared to a new one [28].

This paper's contributions are the study of the novel sliding innovation filter (SIF) for SOC estimation, the proposed SIF architecture in a dual setting, and the use of NASA's PCOE B005 dataset to estimate the LiB's capacity at the end of each cycle throughout its lifetime. The performance of the dual-SIF is compared against a traditional filter in a dual setting, namely the well-known Kalman filter (KF). Artificial measurements are generated for each state by making use of the measurement equations and the battery model equations, resulting in a linear battery model. The artificial measurements allow us to fine tune the SIF's delta, exploiting the potential of the SIF.

This paper is structured as follows: Section 2 presents the battery models used. Section 3 details the experimental dataset used. Section 4 describes the SOC estimation algorithms namely, Ampere-Hour counting method, KF, SIF, and the dual-filter architectures. Section 5 presents the artificial measurement equations used for generating individual measurements for each state from sensor data. Section 6 shows the parameter identification algorithms used for identifying the model's parameter values. Section 7 outlines the experiment results using both dual filters. Section 7 presents the concluding arguments of this paper.

2. Battery Models

This section presents the battery models used for simulation.

2.1. Dual Polarity Model

In the absence of current, the battery's output voltage shows different short time and longtime transient behaviors. These transient behaviors are accurately captured by a two RC branch ECM as opposed to a single RC branch [18]. Furthermore, the use of more than 2 RC branches may be slightly beneficial in terms of accuracy; however, it increases computational time. The dual polarity (DP) model provides a balanced ECM in terms of computational cost and accuracy. The DP model is composed of a voltage source, a resistance and two RC branches, which represents the LiB's OCV as a function of SOC, internal resistance, and the concentration polarization and electrochemical polarization, respectively [18]. In other terms, the voltage source represents the energy inside the battery, the resistance, R_0, represents the loss of energy during operation and the RC branches capture the transient response of the LiB during the transfer of power to/from the battery, that is the electrochemical and concentration polarization. The terminal voltage of the battery is the voltage represented by U_L and the current demanded/supplied to the battery is represented by I_L. Figure 1 shows a schematic of the battery model [18].
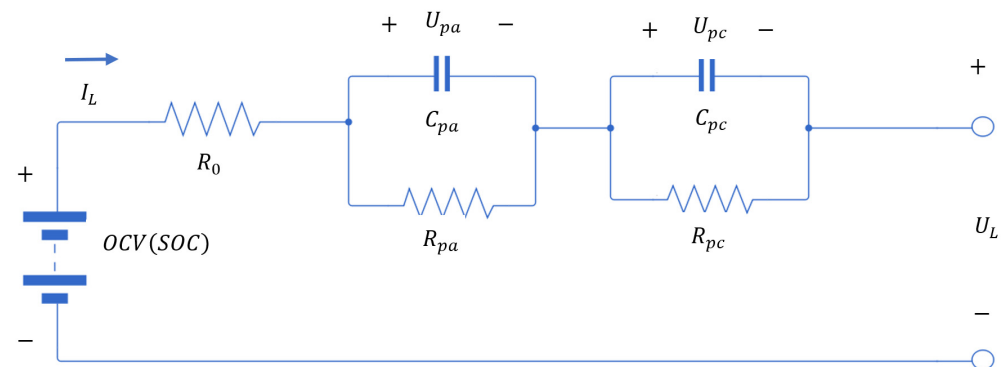
Figure 1. Dual polarity model schematic [18].

After some mathematical analysis, it can be shown that the model can be represented by two differential equations. In (1), the states of the model are the voltage across each RC branch represented by U_{pa} and U_{pc}. Furthermore, the terminal voltage or output equation can be described by (2) [18]:

$$\begin{bmatrix} U_{pa,\,k+1} \\ U_{pc,\,k+1} \end{bmatrix} = \begin{bmatrix} e^{-\frac{\Delta t}{R_{pa}C_{pa}}} & 0 \\ 0 & e^{-\frac{\Delta t}{R_{pc}C_{pc}}} \end{bmatrix} \begin{bmatrix} U_{pa,\,k} \\ U_{pc,\,k} \end{bmatrix} + \begin{bmatrix} R_{pa}\left(1 - e^{-\frac{\Delta t}{R_{pa}C_{pa}}}\right) \\ R_{pc}\left(1 - e^{-\frac{\Delta t}{R_{pc}C_{pc}}}\right) \end{bmatrix} I_L, \quad (1)$$

$$U_{L,\,k+1} = U_{ocv}(SOC_{k+1}) - U_{pa,k+1} - U_{pc,k+1} - I_{L,k}R_0 \tag{2}$$

where a positive I_L discharges the battery.

2.2. Parameter Model

Assuming the LiB's parameters vary slowly (e.g., minutes to hours), the parameter changes during operation and the LiB's aging can be represented by perturbing the states with low levels of white noise. The following equations depict the parameter model.

$$\theta_{k+1} = \theta_k + w_{\theta k}, \tag{3}$$

$$y_{\theta k} = h(x_k,\, u_k,\, \theta_k) + v_{\theta k}, \tag{4}$$

$$w_\theta \;\sim\; N(0, Q_\theta), \tag{5}$$

$$v_\theta \;\sim\; N(0, R_\theta), \tag{6}$$

Here, θ represents the parameter vector, w_θ represents the level of white noise perturbation for each state with covariance Q_θ.

3. Experimental Dataset and Estimation Methods

3.1. B005 Dataset

The PCoE published the Prognostic Data Repository which contains various types of battery datasets intended to aid in the advancement of prognostic algorithms. Among these datasets is the PCoE battery dataset, which provides cycling data of about 38 commercial cells [29]. All these cells had a designed capacity of 2 Ah and were cycled to 70% or 80% of their initial capacity under different temperatures [29]. Each dataset includes time, current, voltage, and temperature measurements for each cycle. As well as impedance data and a date stamp.

This paper selected the B005 dataset to test the dual filters. This dataset contains about 340 discharge and charge cycles or about 615 cycles if the impedance data is accounted for. The battery has an initial capacity of 1.856 Ah and is cycled to 1.303 Ah. The data was resampled from 3 s to 0.6 s to allow for better adherence of the algorithms. Figure 2 depicts the battery capacity degradation over the 615 cycles.

3.2. Ampere Hour Counting

As discussed in Section I, this technique is one of the most popular for determining battery SOC. The SOC is tracked based on the demanded/supplied current from/to the battery. The accuracy of this method is highly dependent on the current measurement and the initial SOC value [30]. Bias in the measurement reading could result in a drift between the estimated SOC and the true value. The following formula depicts this method [30]:

$$SOC = SOC_0 - \frac{\eta_i}{C_n} \int_{t_0}^{t} I_s \, d\tau, \tag{7}$$

where, SOC_0 is the initial SOC, C_n is the nominal capacity of the battery, I_s is the discharge current, η_i represents the correcting factor and i refers to the charge or discharge cycle. In this paper, the charge and discharge cycles are assumed to be the same. Hence, the hysteresis effect of the battery will be neglected and η_i was set to 1.
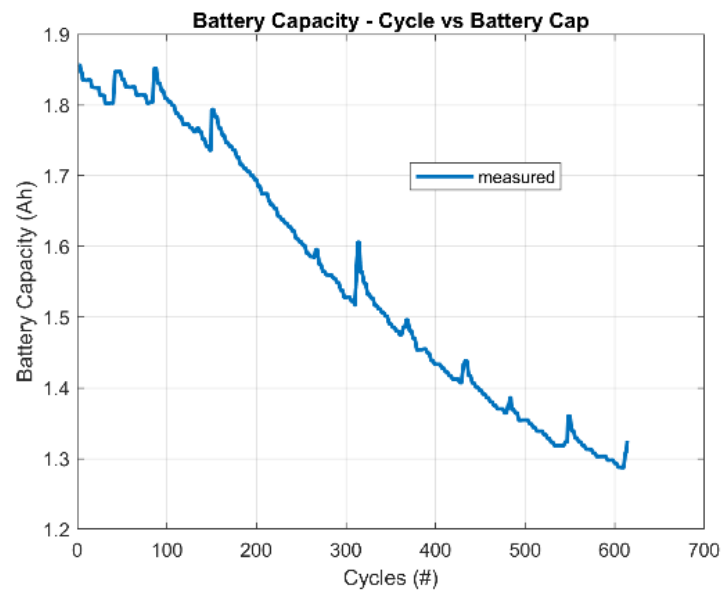
Figure 2. Measured Battery Capacity at the end of each discharge cycle [29].

3.3. Kalman Filter (KF)

A novel recursive solution to linear discrete-data filtering problems was described in 1960 by R.E. Kalman [31]. For a known linear system in the presence of white, Gaussian noise, the Kalman filter (KF) yields the optimal solution by minimizing the state estimation error [31]. The linear system dynamics and measurement model may be described, respectively, by the following two equations [32]:

$$x_{k+1} = Ax_k + Bu_k + w_k, \tag{8}$$

$$z_{k+1} = Cx_{k+1} + v_{k+1}, \tag{9}$$

where A is the dynamics matrix, B is the input matrix, C is the output matrix, x is the system states, z is the measurement output, u is the input, w is the system noise, and v is the measurement noise.

The KF algorithm can be summarized in two stages: prediction and update [33]. Equations (10) and (11) represent the prediction stage, where the update stage consists of (12) through (14).

$$\hat{x}_{k+1|k} = A\hat{x}_{k|k} + Bu_k, \tag{10}$$

$$P_{k+1|k} = AP_{k|k}A^T + Q, \tag{11}$$

$$K_{k+1} = P_{k+1|k}C^T\left[CP_{k+1|k}C^T + R\right]^{-1}, \tag{12}$$

$$\hat{x}_{k+1|k+1} = \hat{x}_{k+1|k} + K_{k+1}\left(z_{k+1} - C\hat{x}_{k+1|k}\right), \tag{13}$$

$$P_{k+1|k+1} = [I - K_{k+1}C]P_{k+1|k}(I - K_{k+1}C)^T + K_{k+1}RK_{k+1}^T, \tag{14}$$

where Q and R are the system and measurement noise covariance matrices, respectively.

3.4. Sliding Innovation Filter

The sliding innovation filter (SIF) is similar to the KF and (8) and (9) are applicable. Both filters were derived using a predictor-corrector architecture where the objective is to reduce the state estimates error and covariances using measurements. The prediction stage of the filter is the same as the KF as per (10) and (11); however, the main difference between the two is how the gain was derived [34].

Unlike the Kalman gain that uses the state error covariance matrix, the SIF gain makes use of the measurement matrix, the innovation term, and a sliding boundary layer [34]. A

time-varying layer was derived in [35]. It is still recommended to calculate for the state error covariance as it contains useful information regarding the estimation error in the filtering process. In simple words, the SIF gain drives the state estimates within the defined boundary layer and pushes the states estimates to switch about the true trajectory [34]. The following are the set of update equations for the SIF [34]:

$$K_{k+1} = C^+ \overline{sat}\left(\left|\widetilde{z}_{k+1|k}\right|/\delta\right), \tag{15}$$

$$\hat{x}_{k+1|k+1} = \hat{x}_{k+1|k} + K_{k+1}\widetilde{z}_{k+1|k}, \tag{16}$$

$$P_{k+1|k+1} = (I - K_{k+1}C_{k+1})P_{k+1|k}(I - K_{k+1}C_{k+1})^T + K_{k+1}\,R\,K_{k+1}^T \tag{17}$$

Note that C^+ refers to the pseudoinverse of C, $\overline{sat}$ refers to the diagonal of the saturation term (value between -1 and $+1$), δ is the sliding boundary layer width. The pseudoinverse is calculated using the Moore-Penrose pseudoinverse. If the inverse of the matrix C exists, performing the pseudoinverse results in a more computational expensive process to calculate the inverse of the matrix.

3.5. Dual Filters: Dual-KF and Dual-SIF

In LiB literature, it has been shown that LiB's capacity degrades overtime as it is subject to deep discharging cycles, full charging cycles or regular use [30]. In addition, LiB behave with a different battery capacity under different operating environments [30]. For both cases, the battery model's capacity would have to be updated to ensure accurate SOC estimation—if the Ampere-Hour Counting method were to be implemented.

Dual filters seek to address the above problem dynamically by connecting two filters [36]. In LiB literature, among the popular dual strategies is the Dual-extended Kalman filter (Dual-EKF) which have been applied to SOC estimation [36]. The EKF is a version of the Kalman filter that can be implemented for nonlinear system. The Dual-EKF strategy uses two EKF algorithms, one for updating the battery model's parameters and the other for SOC estimation. In simple words, the objective of the two filters is to increase the estimation accuracy by allowing the battery parameters to change overtime [36].

The following set of equations summarize the Dual-EKF algorithm for SOC estimation [36]. Equations (18) and (19) are the prediction equations for the state filter, and (20) and (21) are for the parameter filter. Equation (22) through (24) are the update equations for the state filter, and (25) through (27) are for the parameter filter.

$$\hat{x}_{k+1|k} = f\left(\hat{x}_{k|k},\,u_k\right), \tag{18}$$

$$P_{x,k+1|k} = \hat{A}_{x,k}P_{x,k|k}\hat{A}_{x,k}^T + Q_x, \tag{19}$$

$$\hat{\theta}_{k+1} = \hat{\theta}_k, \tag{20}$$

$$P_{\theta,k+1|k} = P_{\theta,k|k} + Q_\theta, \tag{21}$$

$$K_{x,k+1} = P_{x,k+1|k}\,\hat{C}_{x,k+1}^T\left[\hat{C}_{x,k}P_{x,k+1|k}\hat{C}_{x,k+1}^T + R_x\right]^{-1} \tag{22}$$

$$\hat{x}_{x,k+1|k+1} = \hat{x}_{x,k+1|k} + K_{x,k+1}\left[z_{k+1} - h\left(\hat{x}_{x,k+1|k},\,u_{k+1},\hat{\theta}_k\right)\right] \tag{23}$$

$$P_{x,k+1|k+1} = \left[I - K_{x,k+1}\hat{C}_{x,k+1}\right]P_{x,k+1|k} \tag{24}$$

$$K_{\theta,k+1} = P_{\theta,k+1|k}\,\hat{C}_{\theta,k+1}^T\left[\hat{C}_{\theta,k}P_{\theta,k+1|k}\hat{C}_{\theta,k+1}^T + R_\theta\right]^{-1} \tag{25}$$

$$\hat{\theta}_{k+1|k+1} = \hat{\theta}_{k+1|k} + K_{\theta,k+1}\left[z_{k+1} - h\left(\hat{x}_{\theta,k+1},\,u_{\theta,k+1},\hat{\theta}_k\right)\right] \tag{26}$$

$$P_{\theta,k+1|k+1} = \left[I - K_{\theta,k+1}\hat{C}_{\theta,k+1}\right]P_{\theta,k+1|k} \tag{27}$$

where the nonlinearities of the state filter can be linearized. Furthermore, $\hat{C}_{\theta,k}$ refers to the total differential of (4). The following set of equations describe the result [25]:

$$\hat{C}_{\theta,k} = \left. \frac{\mathrm{d}h\left(\hat{x}_{k+1|k},\ u_k,\ \theta_k\right)}{\mathrm{d}\theta_k} \right|_{\theta_{k+1} = \hat{\theta}_{k+1|k}}, \tag{28}$$

$$\frac{\mathrm{d}h\left(\hat{x}_{k+1|k},\ u_{k+1},\ \hat{\theta}_{k+1|k}\right)}{\mathrm{d}\hat{\theta}_{k+1|k}} = \frac{\partial h\left(\hat{x}_{k+1|k},\ u_{k+1},\ \hat{\theta}_{k+1|k}\right)}{\partial \hat{\theta}_{k+1|k}} + \frac{\partial h\left(\hat{x}_{k+1|k},\ u_{k+1},\ \hat{\theta}_{k+1|k}\right)}{\partial \hat{x}_{k+1|k}} \frac{\mathrm{d}\hat{x}_{k+1|k}}{\mathrm{d}\hat{\theta}_{k+1|k}}, \tag{29}$$

$$\frac{\mathrm{d}\hat{x}_{k+1|k}}{\mathrm{d}\hat{\theta}_{k+1|k}} = \frac{\partial f\left(\hat{x}_{k|k+1},\ u_k,\ \hat{\theta}_{k+1|k}\right)}{\partial \hat{\theta}_{k+1|k}} + \frac{\partial h\left(\hat{x}_{k|k+1},\ u_k,\ \hat{\theta}_{k+1|k}\right)}{\partial \hat{x}_{k|k}} \frac{\mathrm{d}\hat{x}_{k|k+1}}{\mathrm{d}\hat{\theta}_{k+1|k}}, \tag{30}$$

$$\frac{\mathrm{d}\hat{x}_{k|k+1}}{\mathrm{d}\hat{\theta}_{k|k}} = \frac{\mathrm{d}\hat{x}_{k|k}}{\mathrm{d}\hat{\theta}_{k|k+1}} - K_{x,k} \frac{\mathrm{d}h\left(\hat{x}_{k|k},\ u_k,\ \hat{\theta}_{k|k+1}\right)}{\mathrm{d}\hat{\theta}_{k|k+1}} \tag{31}$$

where $K_{x,k}$ has little impact to the parameter estimates, thus it can be neglected [25]. Removing the right term in (31), reduces the equation to $\frac{\mathrm{d}\hat{x}_{k|k}}{\mathrm{d}\hat{\theta}_{k|k+1}}$ which can now be estimated by recursion with an initial value of $\frac{\mathrm{d}\hat{x}_{k|k+1}}{\mathrm{d}\hat{\theta}_{k|k}} = 0$ [25].

4. Artificial Measurements

This section presents the state measurement equations derived using the output equation. It is important to note that by making use of the equations derived in this section, the output equation has been linearized and can be represented as in (13). In other words, the outputs (23) and (26) can be written as (13).

4.1. State Measurement Equations

The state measurement equations were derived to allow the SIF access to individual δ for each state. The two measurements for this system are the current I_s and the terminal voltage U_L. From the terminal voltage Equation (2), one can derive individual measurements for each state and R_0. The following are the derived state measurement equations:

$$\hat{U}_{pa,k+1} = OCV(SOC_k) - U_{L,k+1} - R_{0,k}I_{s,k} - U_{pc,k}, \tag{32}$$

$$\hat{U}_{pc,k+1} = OCV(SOC) - U_{L,k+1} - R_{o,k}I_{s,k} - U_{pa,k}, \tag{33}$$

$$\hat{SOC}_{k+1} = OCV^{-1}\left(U_{L,k+1} + U_{pa,k} + U_{pc,k} + R_{o,k}I_{s,k}\right) \tag{34}$$

where $\hat{U}_{pa}$, $\hat{U}_{pc}$, and $\hat{SOC}$ are the measurements for each state of the battery model. $OCV^{-1}(\because)$ is the inverse function of $OCV(SOC)$.

4.2. Parameter Measurement Equations

To derive measurements for the parameter model, (2) was used to derive a measurement for R_0 and (7) was used to derive the $Batt_{cap}$ measurement. The equations can be summarized, respectively, as follows:

$$\hat{R}_o = \frac{1}{I_{s,k}}\left[OCV(SOC) - U_L - U_{pa} - U_{pc}\right], \tag{35}$$

$$\hat{Batt}_{Cap} = \frac{\Delta t * I_{s,k}}{abs(3.6 * \Delta SOC_k)}, \tag{36}$$

Figure 3 depicts a block diagram of the dual filter strategy including the measurement equations.
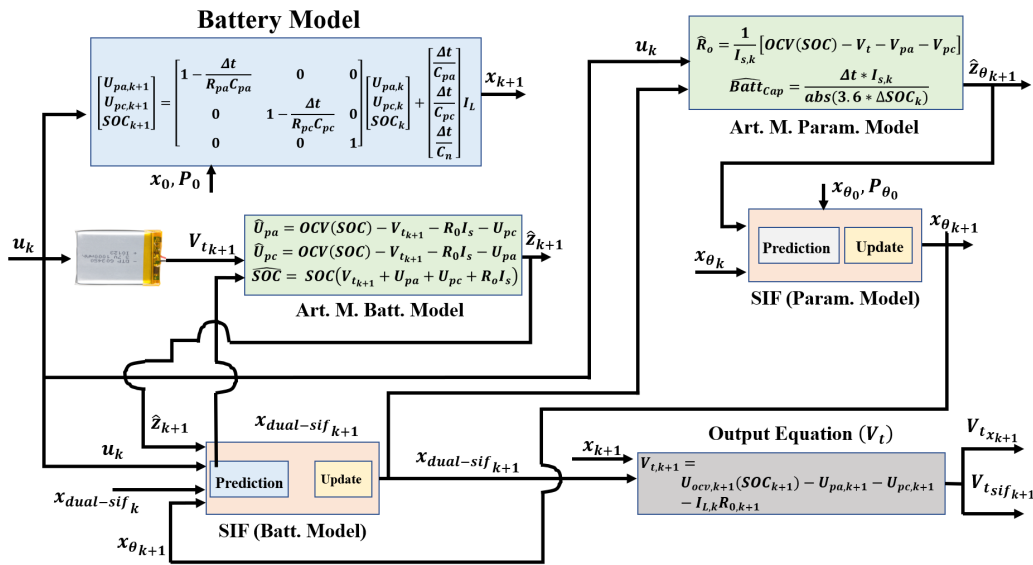
Figure 3. Block diagram of the proposed dual strategy.

5. Parameter Identification

In this section, the nonlinear least squares (NLLS) algorithm is used for parameter identification. After analyzing the DP model described in section II, the parameters to be identified are $OCV(SOC)$, R_0, R_{pa}, C_{pa}, R_{pc}, C_{pc}, $Batt_{cap}$. The dataset already provides the initial $Batt_{cap}$ at 1.856 Ah.

Least Squares

Analyzing the DP model, the required relationship for NLLS between the measurable data and the parameters can be defined as [22]:

$$OCV(SOC) = \alpha_0 + \alpha_1 SOC + \alpha_2 SOC^2 + \alpha_3 SOC^3 + \alpha_4 SOC^4 + \alpha_5 SOC^5, \tag{37}$$

$$U_{pa} = I_L R_{pa}\left(1 - e^{-\frac{t}{R_{pa}C_{pa}}}\right), \tag{38}$$

$$U_{pc} = I_L R_{pc}\left(1 - e^{-\frac{t}{R_{pc}C_{pc}}}\right), \tag{39}$$

$$U_L = OCV(SOC) - I_L R_0 - I_L R_{pa}\left(1 - e^{-\frac{t}{R_{pa}C_{pa}}}\right) - I_L R_{pc}\left(1 - e^{-\frac{t}{R_{pc}C_{pc}}}\right), \tag{40}$$

$$\theta = \left[\alpha_0, \ \alpha_1, \alpha_2, \alpha_3, \alpha_4, \alpha_5, \ R_0, \ R_{pa}, \ \frac{1}{R_{pa}C_{pa}}, \ R_{pc}, \ \frac{1}{R_{pc}C_{pc}}\right], \tag{41}$$

where t is the sampled time vector, the $OCV(SOC)$ curve is approximated as a 5th order polynomial with α_0 equal to 3.27 V which corresponds to the voltage at the end of the first discharge cycle. θ is the parameter vector. The capacitance values are estimated as $1/R_{pc}C_{pc}$ and $1/R_{pa}C_{pa}$ to account for their significantly higher magnitude compared to resistances. It has been reported in the literature that the capacitance values are two to three orders of magnitude higher than the resistance values [22,37].

The *lsqcurvefit* MATLAB® function was used for parameter estimation subject to the boundaries and initial conditions detailed in Table 1. Table 2 summarizes the results from the NLLS method. These parameter values were used across all experiments. The terminal voltage's RMSE between the derived model and the measured data was 0.053. Moreover, Figures 4 and 5 depict the error generated between the NLLS model and the measured data.

Table 1. NLLS Boundaries and initial guess.

Parameters	R_0	R_{pa}	C_{pa}	R_{pc}	C_{pc}
Unit	Ω	Ω	$1/(\Omega F)$	Ω	$1/(\Omega F)$
LB	0.001	0.01	0.0001	0.01	0.01
UB	0.500	0.50	0.0020	0.50	0.10
Guess	0.020	0.10	0.0010	0.10	0.01

Table 2. NLLS parameter estimation results.

RC-Parameters	Value	OCV(SOC)	Value
R_0	0.065	α_1	2.94
R_{pa}	0.0615	α_2	−5.66
C_{pa}	1860	α_3	2.70
R_{pc}	0.0227	α_4	3.84
C_{pc}	146825	α_5	−2.94
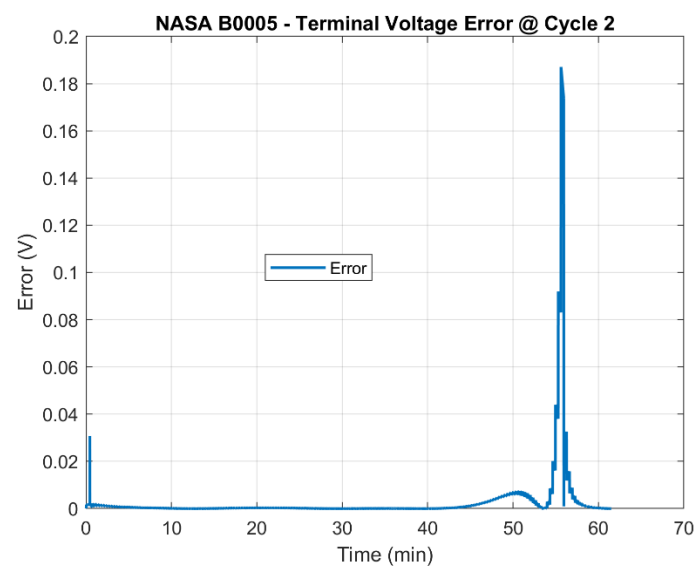
Figure 4. LS Model Error Squared: Terminal Voltage.
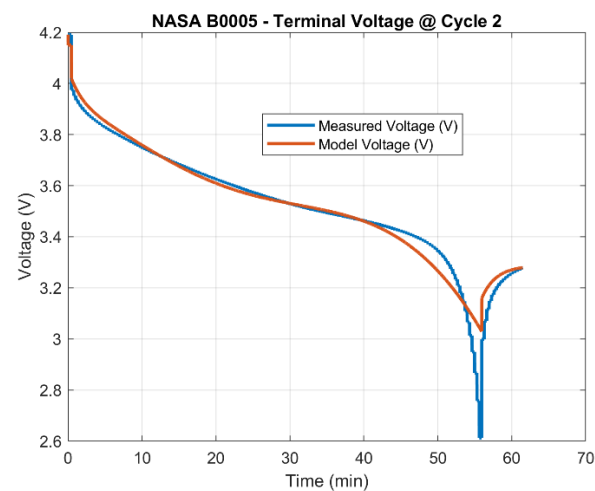
Figure 5. Model vs. Measured Voltage.

Lastly, Figure 6 depicts the obtained SOC-OCV curve, and (42) illustrates the *OCV(SOC)* equation.

$$OCV_{Lipo_{Avg}} = @(SOC)\left(-2.94\,SOC^5 + 3.84\,SOC^4 + 2.7\,SOC^3 - 5.67\,SOC^2 + 2.94\,SOC + 3.27\right), \tag{42}$$
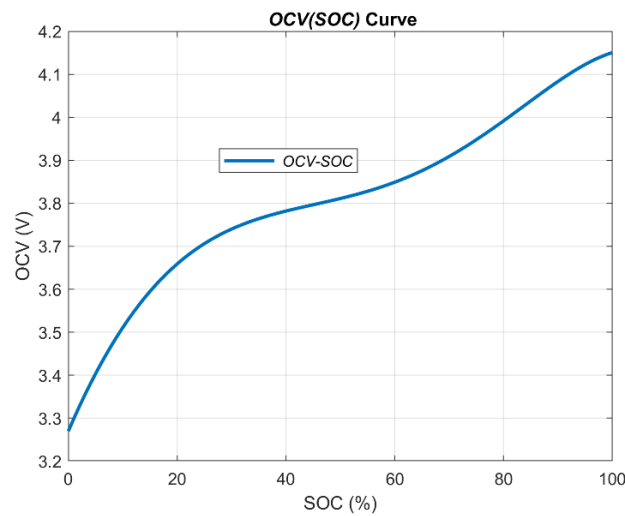
Figure 6. SOC-OCV Curve Plot.

6. Experimental Results and Discussion

This section details the experimental results obtained by both Dual-filter strategies: Dual-KF and Dual-SIF.

6.1. SOC Estimation: 10th Cycle and 400th Cycle

This section presents the *SOC* estimation results using the B005 dataset and the dual filter algorithms. Table 3 summarizes the initial conditions used for the experiment.

Table 3. Initialization values for both filters: Dual-KF/Dual-SIF.

Variable	Battery Model	Parameter Model
V_{pa}	0	0.065 Ω
V_{pc}	0	2 Ah
SOC	100%	-
Q	Diag $(5 \times 10^{-5}, 3 \times 10^{-5}, 5 \times 10^{-7})$	Diag $(5 \times 10^{-7}, 1 \times 10^{-8})$
R	Diag $(0.1, 0.01, 1)$	Diag $(10, 1)$
Delta	$[10; 7; 2000]$	$[450; 90]$

The filter making use of the battery model was initialized to represent a relaxed and fully charged battery. The final Q matrix values were chosen after running the experiment several times and analyzing the resulting plots of each state at the end of the simulation. The R matrix values were set based on the measurement data.

The second filter, making use of the parameter model, was initialized based on the parameter identification values. The filter is only allowed to make changes to the internal resistance, R_0, and battery capacity, Bat_{cap}, parameters, which are critical markers of a healthy battery. The values for Q were selected based on how much change was allowed for each parameter.

Figure 7 illustrates the terminal voltage and *SOC* estimation results at the 10th Cycle. This cycle is a discharge cycle starting with a 100% *SOC* to 0% *SOC*. Part (a) of the figure illustrates a correct terminal voltage estimation compared to the model results in Figure 5. Furthermore, the SOC results shown on parts (b) and (c) depict a full discharge of the battery using (7). As shown in Figure 7, the battery model and parameter model derived can accurately capture the behavior of the battery in conjunction with the KF and SIF.

Figure 8 shows the terminal voltage, and *SOC* estimation results of the battery at the 600th Cycle. Similar to the 10th cycle, this cycle is a discharge cycle; however, the battery has significantly aged. The new Bat_{cap} is around 1.3 Ah compared to 1.86 Ah—about a 30% reduction. Part (a) of this figure illustrates accurate terminal voltage results for both filters,

showing that both filters have adapted to the new conditions. Part (b) shows the *SOC* estimation results of the initial model using the dynamics of a new battery, no updates to the parameters, and the SOC results of both filters. The filters correctly deplete the battery, meaning that the parameter of the model have been updated successfully. Furthermore, it can be seen that the battery is fully depleted before the 40th minute which is also reflective of the terminal voltage in (a). Part (c) illustrates the artificial measurements generated for *SOC*.

(**a**)

(**b**)

(**c**)
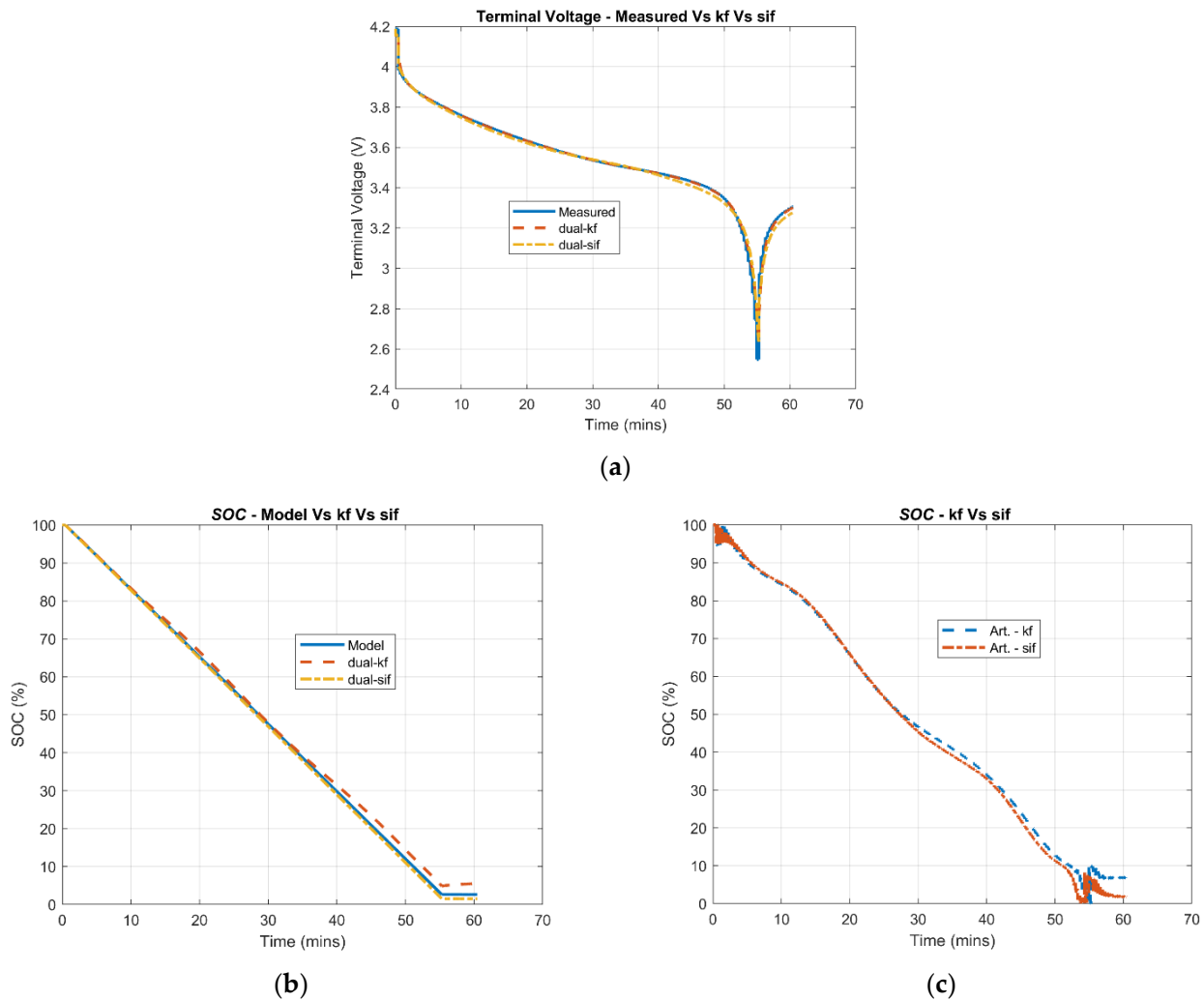
Figure 7. 10th Cycle Results: (**a**) Terminal Voltage, (**b**) SOC Estimate, (**c**) SOC Artificial Measurement.

6.2. Battery Capacity Estimation: Dual KF and Dual SIF

This section presents the battery capacity estimation results from both filters using the B005 dataset. The algorithms were initialized as in Table 3.

Based on the first battery capacity measurement provided by the dataset, the starting capacity of the battery was measured at 94% of the manufacturer's datasheet (2 Ah). Both filters should account for this starting battery capacity during the estimation process. Figure 9 depicts the Bat_{cap} and R_0 estimation at the end of each cycle. As the battery ages, it is expected for its capacity to degrade, Bat_{cap}, and its internal resistance, R_0, to increase. Both filters show good profiles and estimation results; however, the KF mimics more accurately the measured data's trend. Table 4 shows the RMSE values for the battery capacity estimate and terminal voltage estimate of both filters. Both filters show good results; however, the dual-KF performs slightly better than the dual-SIF.

(a)

(b)

(c)
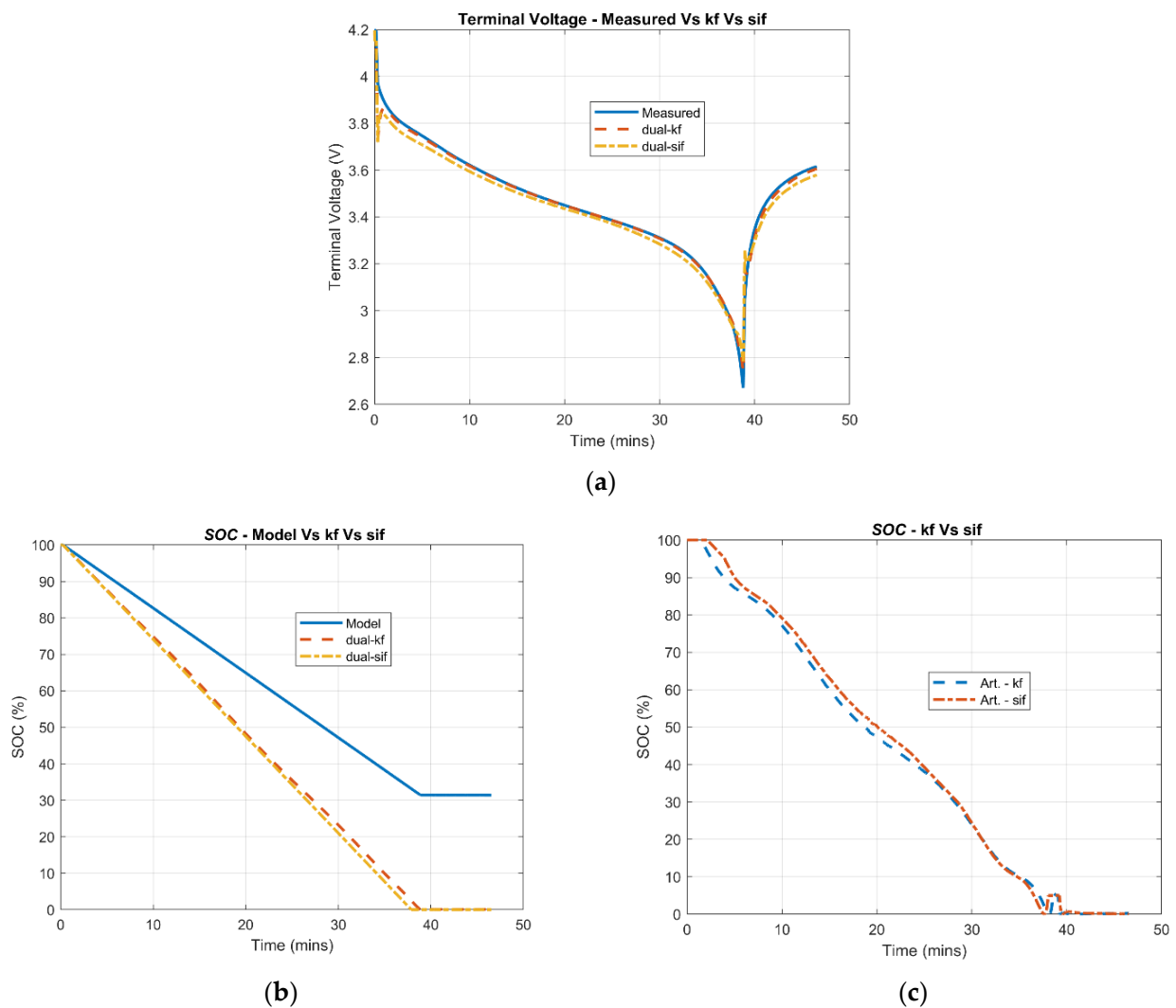
Figure 8. 600th Cycle Estimation Results: (**a**) Terminal Voltage, (**b**) *SOC* Estimate, (**c**) *SOC* Artificial Measurement.

Table 4. RMSE Results.

Output/State	Dual-KF	Dual-SIF
Bat_{cap}	0.0283	0.0342
Terminal Voltage	0.0227	0.0398

6.3. Battery Capacity Estimation under Fault: Jump in Data

This section shows the results generated using a shorten data by jumping from cycle 150 to cycle 450. Both filters should converge to the new battery dynamics—aged battery.

Based on the measured battery capacity at the 450th cycle the "true" Bat_{cap} should be at 1.39 Ah. Both filters, should account for this sudden drop in battery capacity. Furthermore, the filters should significantly increase the internal resistance. Figure 10 illustrates the estimation results of both filters. It is evident, that both filets converge to the "true" Bat_{cap}; however, the dual-SIF shows faster convergence than the dual-KF. This rate of convergence is also evident in Part A.
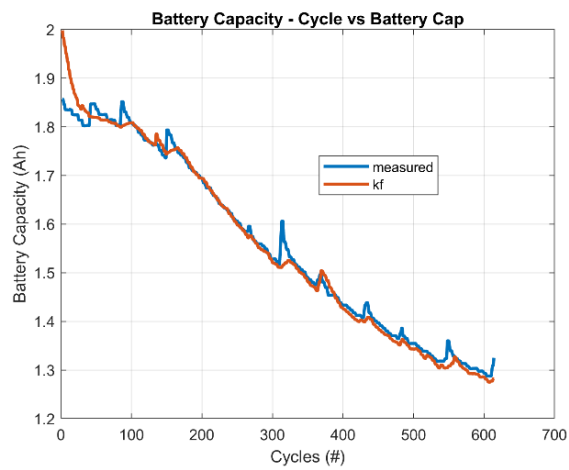
(**a**)
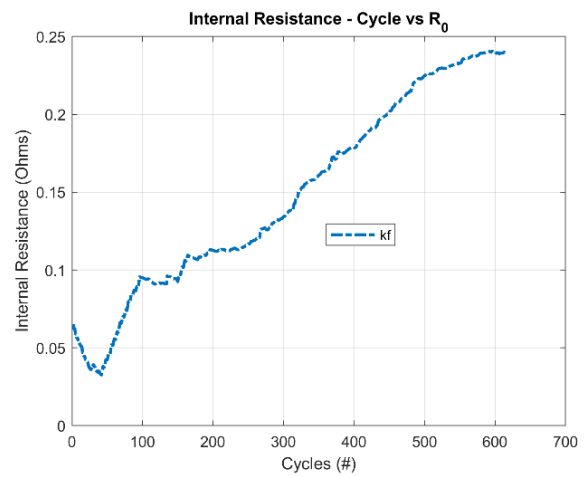
(**b**)
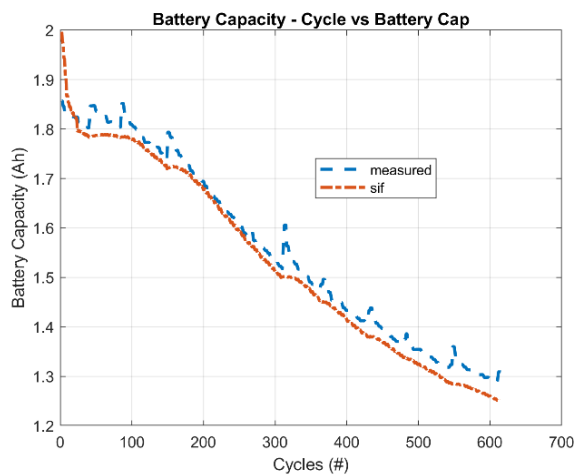
(**c**)
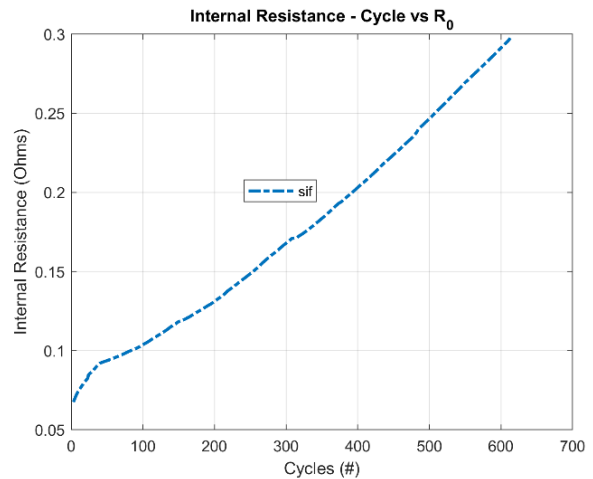
(**d**)

Figure 9. Dual Estimation: (**a**) Dual-KF Battery Capacity Estimation. (**b**) Dual-KF Internal Resistance Estimation. (**c**) Dual-SIF Battery Capacity Estimation. (**d**) Dual-SIF Internal Resistance Estimation.

Table 5 presents the RMSE results for both filters. The dual-SIF has a better RMSE due to the faster convergence rate than the dual-KF. Moreover, the dual-SIF has a better RMSE value estimating the terminal voltage as it makes use of the correct battery capacity at earlier cycles.

Table 5. RMSE Results for both filters.

Output/State	Dual-KF	Dual-SIF
Bat_{cap}	0.1233	0.0675
Terminal Voltage	0.0776	0.0460
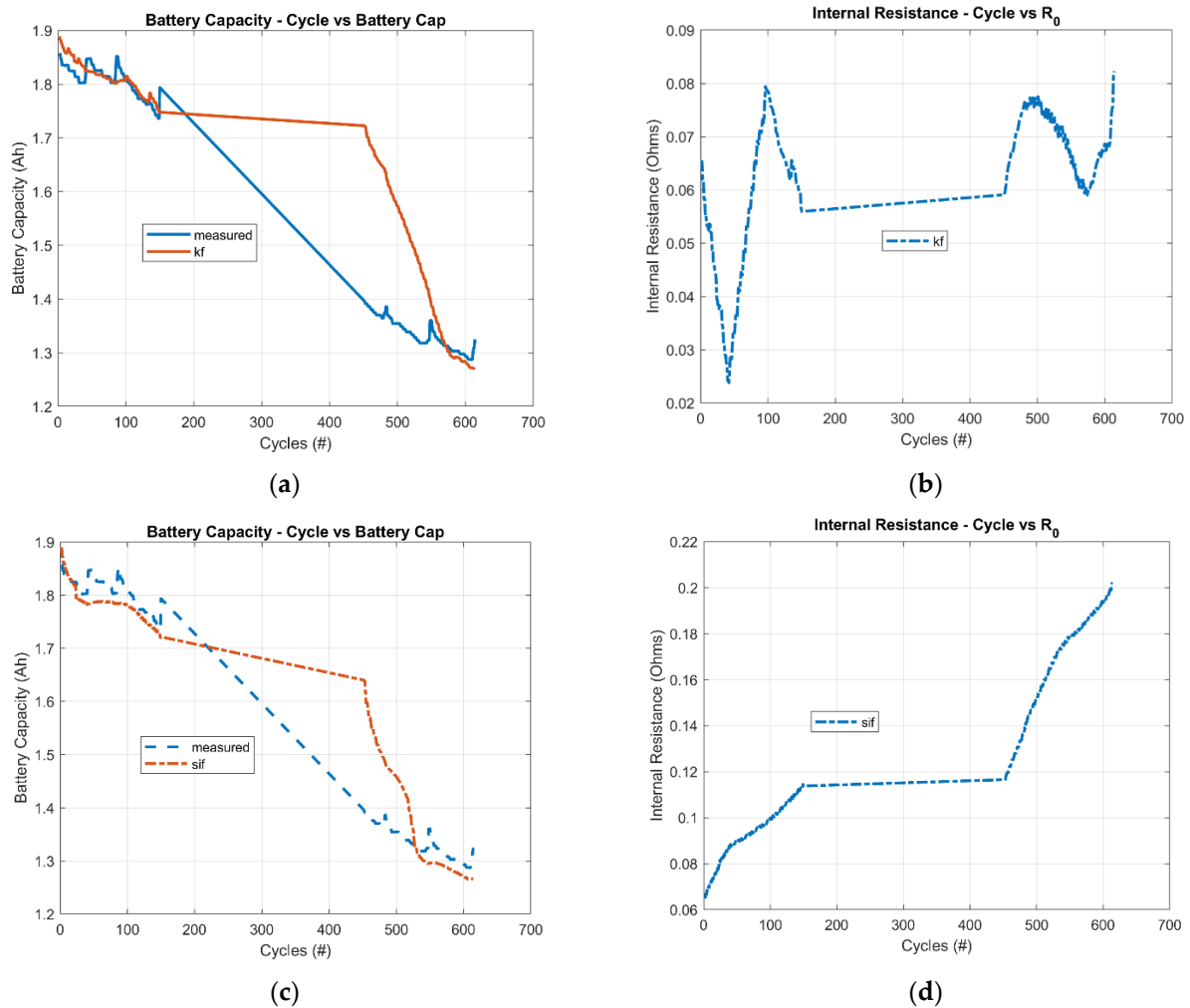
Figure 10. (**a**) Dual-KF Battery Capacity Estimation. (**b**) Dual-KF Internal Resistance Estimation. (**c**) Dual-SIF Battery Capacity Estimation. (**d**) Dual-SIF Internal Resistance Estimation.

7. Conclusions

In this paper, the sliding innovation filter and Kalman filter were implemented to estimate the SOC of a lithium-ion battery. Moreover, the sliding innovation filter and Kalman filter were also implemented using a dual strategy to estimate a lithium-ion battery's capacity under cycling. The experimental data used was NASA's PCOE B005 dataset, which provides cycling data of a 2 Ah lithium-ion battery until retirement (1.3 Ah) for the purpose of advancing prognostic algorithms. This experimental data was fed to the algorithms, and the estimation results of both dual filters were compared to the dataset's measured battery capacity at the end of each discharge cycle. Lastly, this paper makes use of artificial measurement equations to generate individual measurements for each state.

The terminal voltage and *SOC* estimation results from the 10th and 600th cycles demonstrate good performance of both dual filter algorithms when the battery is at a healthy state and as the battery aged. These results showed that both algorithms updated the model accordingly and depleted the battery at the correct times, which can be corroborated by analyzing the terminal voltage plots. Moreover, the low RMSE values for battery capacity estimation show good accuracy for both filters, with the Kalman filter having a better profile trend and the sliding innovation filter resulting in a smoother curve.

Lastly, the proposed dual sliding innovation filter and the Kalman filter were tested under rapid changing dynamics. The dataset was shortened by cutting the data from the 150th to the 450th cycle. The simulation results demonstrated that the dual sliding inno-

vation filter has a faster convergence to the new battery dynamics than the dual Kalman filter, resulting in lower RMSE values in battery capacity and terminal voltage estimation. This faster rate of convergence suggests that the sliding innovation filter may adapt better to more aggressive changes in battery dynamics than the Kalman filter; however, further study should be done comparing both algorithm responses to different degrees of changing dynamics. Future work will look at performing a comprehensive comparison with nonlinear estimation methods on an experimental setup currently under development.

References

1. Li, X.; Sun, X.; Hu, X.; Fan, F.; Cai, S.; Zheng, C.; Stucky, G.D. Review on comprehending and enhancing the initial Coulombic efficiency of anode materials in lithium-ion/sodium-ion batteries. *Nano Energy* **2020**, *77*, 105143. [CrossRef]
2. Zheng, L.; Zhu, J.; Wang, G.; Lu, D.D.-C.; He, T. Lithium-ion Battery Instantaneous Available Power Prediction Using Surface Lithium Concentration of Solid Particles in a Simplified Electrochemical Model. *IEEE Trans. Power Electron.* **2018**, *33*, 9551–9560. [CrossRef]
3. IEEE Electronics Packing Society; Institute of Electrical and Electronics Engineers. Resistive Sensors Network Analog Multiplexing. In Proceedings of the 2018 IEEE 24th International Symposium for Design and Technology in Electronic Packaging (SIITME): IEEE Xplore Compliant Proceedings, Iasi, Romania, 25–28 October 2018; Institute of Electrical and Electronics Engineers: Piscataway, NJ, USA, 2018; ISBN 9781538655771.
4. Nizam, H.M.; Maghfiroh, R.; Rosadi, A.; Kusumaputri, K.D.U. IEEE Staff. In Proceedings of the 2019 6th International Conference on Electric Vehicular Technology (ICEVT), Bali, Indonesia, 18–21 November 2019; IEEE: Piscataway, NJ, USA, 2019; ISBN 9781728129174.
5. Ouyang, D.; Weng, J.; Chen, M.; Liu, J.; Wang, J. Experimental analysis on the degradation behavior of overdischarged lithium-ion battery combined with the effect of high-temperature environment. *Int. J. Energy Res.* **2020**, *44*, 229–241. [CrossRef]
6. Feng, L.; Ding, J.; Han, Y. Improved sliding mode based EKF for the SOC estimation of lithium-ion batteries. *Ionics* **2020**, *26*, 2875–2882. [CrossRef]
7. Zhang, S.; Sun, H.; Lyu, C. A method of SOC estimation for power Li-ion batteries based on equivalent circuit model and extended Kalman filter. In Proceedings of the 2018 13th IEEE Conference on Industrial Electronics and Applications (ICIEA), Wuhan, China, 31 May–2 June 2018; Institute of Electrical and Electronics Engineers Inc.: Piscataway, NJ, USA, 2018; pp. 2683–2687.
8. Luo, J.; Peng, J.; He, H. Lithium-ion battery SOC estimation study based on Cubature Kalman filter. *Energy Procedia* **2019**, *158*, 3421–3426. [CrossRef]
9. He, H.; Qin, H.; Sun, X.; Shui, Y. Comparison Study on the Battery SoC Estimation with EKF and UKF Algorithms. *Energies* **2013**, *6*, 5088–5100. [CrossRef]
10. How, D.N.T.; Hannan, M.A.; Hossain Lipu, M.S.; Ker, P.J. State of Charge Estimation for Lithium-Ion Batteries Using Model-Based and Data-Driven Methods: A Review. *IEEE Access* **2019**, *7*, 136116–136136. [CrossRef]
11. Westerhoff, U.; Kurbach, K.; Lienesch, F.; Kurrat, M. Analysis of Lithium-Ion Battery Models Based on Electrochemical Impedance Spectroscopy. *Energy Technol.* **2016**, *4*, 1620–1630. [CrossRef]
12. Tran, N.-T.; Khan, A.B.; Nguyen, T.-T.; Kim, D.-W.; Choi, W. SOC Estimation of Multiple Lithium-Ion Battery Cells in a Module Using a Nonlinear State Observer and Online Parameter Estimation. *Energies* **2018**, *11*, 1620. [CrossRef]
13. Lai, X.; Qiao, D.; Zheng, Y.; Zhou, L. A Fuzzy State-of-Charge Estimation Algorithm Combining Ampere-Hour and an Extended Kalman Filter for Li-Ion Batteries Based on Multi-Model Global Identification. *Appl. Sci.* **2018**, *8*, 2028. [CrossRef]
14. Institute of Electrical and Electronics Engineers. Predictive Method of Capacitor Production Order Based on ARIMA Model. In Proceedings of the 2018 IEEE 4th International Conference on Control Science and Systems Engineering (ICCSSE), Wuhan, China, 21–23 August 2018; IEEE: Piscataway, NJ, USA, 2018; ISBN 9781538678879.

15. Zhang, C.; Li, K.; Mcloone, S.; Yang, Z. Battery modelling methods for electric vehicles—A review. In Proceedings of the 2014 European Control Conference (ECC), Strasbourg, France, 24–27 June 2014; Institute of Electrical and Electronics Engineers Inc.: Piscataway, NJ, USA, 2014; pp. 2673–2678.

16. Vehicular Technology Society; Truòng đại học bách khoa Hà Nôi; Institute of Electrical and Electronics Engineers. Connect green e-Motion. In Proceedings of the 2019 IEEE Vehicle Power and Propulsion Conference (VPPC), Hanoi, Vietnam, 14–17 October 2019; IEEE: Piscataway, NJ, USA, 2019; ISBN 9781728112497.

17. He, H.; Xiong, R.; Fan, J. Evaluation of Lithium-Ion Battery Equivalent Circuit Models for State of Charge Estimation by an Experimental Approach. *Energies* **2011**, *4*, 582–598. [CrossRef]

18. Eltoumi, F.; Badji, A.; Becherif, M.; Ramadan, H.S. Experimental Identification using Equivalent Circuit Model for Lithium-Ion Battery. *Int. J. Emerg. Electr. Power Syst.* **2018**, *19*, 20170210. [CrossRef]

19. Song, Y.; Park, M.; Seo, M.; Kim, S.W. Improved SOC estimation of lithium-ion batteries with novel SOC-OCV curve estimation method using equivalent circuit model. In Proceedings of the 2019 4th International Conference on Smart and Sustainable Technologies (SpliTech), Split, Croatia, 18–21 June 2019.

20. China Power Supply Society; IEEE Power Electronics Society; Power Sources Manufacturers Association; Institute of Electrical and Electronics Engineers. The state-of-the-art in power electronics, energy conversion and its applications. In Proceedings of the 2018 IEEE International Power Electronics and Application Conference and Exposition (PEAC), Crowne Plaza Shenzhen Longgang City Centre, Shenzhen, China, 4–7 November 2018; IEEE: Piscataway, NJ, USA, 2018; ISBN 9781538660546.

21. Vidal, C.; Malysz, P.; Kollmeyer, P.; Emadi, A. Machine Learning Applied to Electrified Vehicle Battery State of Charge and State of Health Estimation: State-of-the-Art. *IEEE Access* **2020**, *8*, 52796–52814. [CrossRef]

22. IEEE Control Systems Society; IEEE Robotics and Automation Society; Keisoku Jido Seigyo Gakkai (Japan); Institute of Electrical and Electronics Engineers. *Proceedings of the First Annual IEEE Conference on Control Technology and Applications: CCTA 2017, Kohala Coast, HI, USA, 27–30 August 2017*; IEEE: Piscataway, NJ, USA, 2017; ISBN 9781509021826.

23. Xia, B.; Lao, Z.; Zhang, R.; Tian, Y.; Chen, G.; Sun, Z.; Wang, W.; Sun, W.; Lai, Y.; Wang, M.; et al. Online Parameter Identification and State of Charge Estimation of Lithium-Ion Batteries Based on Forgetting Factor Recursive Least Squares and Nonlinear Kalman Filter. *Energies* **2017**, *11*, 3. [CrossRef]

24. Bezha, M.; Nagaoka, N. Online learning ANN model for SoC estimation of the Lithium- Ion battery in case of small amount of data for practical applications. In Proceedings of the 2019 10th International Conference on Power Electronics and ECCE Asia (ICPE 2019-ECCE Asia), Busan, Korea, 27–31 May 2019; IEEE: Piscataway, NJ, USA, 2019.

25. Taborelli, C.; Onori, S. State of charge estimation using extended Kalman filters for battery management system. In Proceedings of the 2014 IEEE International Electric Vehicle Conference (IEVC), Florence, Italy, 17–19 December 2014; Institute of Electrical and Electronics Engineers Inc.: Piscataway, NJ, USA, 2014; pp. 1–8.

26. Wielitzka, M.; Dagen, M.; Ortmaier, T. Joint unscented Kalman filter for state and parameter estimation in vehicle dynamics. In Proceedings of the 2015 IEEE Conference on Control Applications (CCA), Sydney, Australia, 21–23 September 2015; Institute of Electrical and Electronics Engineers Inc.: Piscataway, NJ, USA, 2015; pp. 1945–1950. [CrossRef]

27. Erlangga, G.; Perwira, A.; Widyotriatmo, A. State of charge and state of health estimation of lithium battery using dual Kalman filter method. In Proceedings of the 2018 International Conference on Signals and Systems (ICSigSys), Bali, Indonesia, 1–3 May 2018; Institute of Electrical and Electronics Engineers Inc.: Piscataway, NJ, USA, 2018; pp. 243–248.

28. Liao, Q.; Mu, M.; Zhao, S.; Zhang, L.; Jiang, T.; Ye, J.; Shen, X.; Zhou, G. Performance assessment and classification of retired lithium ion battery from electric vehicles for energy storage. *Int. J. Hydrogen Energy* **2017**, *42*, 18817–18823. [CrossRef]

29. Hasib, S.A.; Islam, S.; Chakrabortty, R.K.; Ryan, M.J.; Saha, D.K.; Ahamed, H.; Moyeen, S.I.; Das, S.K.; Ali, F.; Islam, R.; et al. A Comprehensive Review of Available Battery Datasets, RUL Prediction Approaches, and Advanced Battery Management. *IEEE Access* **2021**, *9*, 86166–86193. [CrossRef]

30. Lai, X.; Wang, S.; He, L.; Zhou, L.; Zheng, Y. A hybrid state-of-charge estimation method based on credible increment for electric vehicle applications with large sensor and model errors. *J. Energy Storage* **2020**, *27*, 101106. [CrossRef]

31. Kalman, R.E. A New Approach to Linear Filtering and Prediction Problems. *J. Basic Eng.* **1960**, *82*, 35–45. [CrossRef]

32. Welch, G.; Bishop, G. *An Introduction to the Kalman Filter*; ACM, Inc.: New York, NY, USA, 2001.

33. Gadsden, S.A.; Habibi, S.; Kirubarajan, T. Kalman and smooth variable structure filters for robust estimation. *IEEE Trans. Aerosp. Electron. Syst.* **2014**, *50*, 1038–1050. [CrossRef]

34. Gadsden, S.A.; Al-Shabi, M. The Sliding Innovation Filter. *IEEE Access* **2020**, *8*, 96129–96138. [CrossRef]

35. Lee, A.S.; Gadsden, S.A.; Al-Shabi, M. An Adaptive Formulation of the Sliding Innovation Filter. *IEEE Signal Process. Lett.* **2021**, *28*, 1295–1299. [CrossRef]

36. Nejad, S.; Gladwin, D.; Stone, D. A systematic review of lumped-parameter equivalent circuit models for real-time estimation of lithium-ion battery states. *J. Power Sources* **2016**, *316*, 183–196. [CrossRef]

37. Wei, X.; Yimin, M.; Feng, Z. Lithium-ion Battery Modeling and State of Charge Estimation. *Integr. Ferroelectr.* **2019**, *200*, 59–72. [CrossRef]